

Rings and spirals in barred galaxies. II. Ring and spiral morphology.

E. Athanassoula¹, M. Romero-Gómez^{1,2}, A. Bosma¹, J.J. Masdemont³

¹Laboratoire d’Astrophysique de Marseille (LAM), UMR6110, CNRS/Université de Provence, Technopôle de Marseille Etoile, 38 rue Frédéric Joliot Curie, 13388 Marseille Cédex 13, France

²Dep. Astronomia i Meteorologia, Universitat de Barcelona, Martí i Franques 1, 08028 Barcelona, Spain

³I.E.E.C & Dep. Mat. Aplicada I, Universitat Politècnica de Catalunya, Diagonal 647, 08028 Barcelona, Spain

Received

ABSTRACT

In this series of papers, we propose a theory to explain the formation and properties of rings and spirals in barred galaxies. The building blocks of these structures are orbits guided by the manifolds emanating from the unstable Lagrangian points located near the ends of the bar. In this paper we focus on a comparison of the morphology of observed and of theoretical spirals and rings and we also give some predictions for further comparisons. Our theory can account for spirals as well as both inner and outer rings. The model outer rings have the observed R_1 , R'_1 , R_2 , R'_2 and $R_1 R_2$ morphologies, including the dimples near the direction of the bar major axis. We explain why the vast majority of spirals in barred galaxies are two armed and trailing, and discuss what it would take for higher multiplicity arms to form. We show that the shapes of observed and theoretical spirals agree and we predict that stronger non-axisymmetric forcings at and somewhat beyond corotation will drive more open spirals. We compare the ratio of ring diameters in theory and in observations and predict that more elliptical rings will correspond to stronger forcings. We find that the model potential may influence strongly the numerical values of these ratios.

Key words: galaxies – structure – ringed galaxies – barred galaxies

1 INTRODUCTION

The discs of barred galaxies very often have spectacular sub-structures such as grand design spirals, or inner and outer rings. In fact, these sub-structures are observed much more often in barred than in non-barred disc galaxies. Their formation is intimately linked to the evolution of disc galaxies and also gives important information on the corresponding underlying potential and the bar pattern speed. Therefore many efforts, both theoretical and numerical, have been made to explain them (see e.g. Lin 1967, Toomre 1977, Toomre 1981, Athanassoula 1984, Athanassoula & Bosma 1985 and Buta & Combes 1996 for reviews). None of these theories, however, could explain all observed properties and, particularly, none could explain both spirals and rings.

For this reason, we propose in this and in previous papers a new theory to explain all these features in a single theoretical framework. It relies on the dynamics of the unstable Lagrangian points located near the ends of the bar and of the associated manifolds. These guide the motion of the chaotic orbits that constitute the building blocks of the spirals and rings. Our theory and its applications are described in five papers. The first two (Romero-Gómez *et al.* 2006, hereafter Paper I; Romero-Gómez *et al.* 2007, hereafter Paper II) contain most of the theoretical groundwork. They describe in detail the dynamics of the region around the two unstable Lagrangian points and of the corresponding manifolds. A theory, however, can be dynami-

cally correct but still irrelevant to a particular application. Thus, the aim of the remaining three papers is to check whether our theory is applicable to observed spirals and rings. In Paper III (Athanassoula, Romero-Gómez & Masdemont 2009), we considered the orbits guided by the manifolds as potential building blocks for spiral and rings and derived their relevant properties. In this paper, the fourth of this series, we compare the morphology of observed and of theoretical spirals and rings to test whether there is agreement. We also make a number of predictions based on our theory, which can be tested with future observations. In Paper V (Athanassoula *et al.* 2009b, to be submitted), the last of this series, we will present further comparisons with observations. These last three papers can be considered as one entity and therefore have the same main title (“Rings and spirals in barred galaxies”), but we will always consider them as part of the whole series and refer to them as Papers III, IV and V, respectively.

The comparisons between our theory and the observations have, by necessity, to be qualitative. Indeed, in all our calculations we have used three specific families of analytic potentials. These can not cover all possible forms of observed barred galaxy potentials, nor are we sure that they share all their relevant properties. Furthermore, we do not take into account self-gravity, i.e. we neglect the potential of the structure itself. If a given quantity depends considerably on the properties of the potential, we may not find good quantitative agreement between our theoretical results

arXiv:0910.0757v1 [astro-ph.CO] 5 Oct 2009

and observations, even though our theory is correct and applicable. For example, if the ring extent depends strongly on the potential used, then one can expect discrepancies between the observed and the theoretical extent values, if the adopted potential does not match observations in the relevant regions.

Section 2 contains a brief reminder of the main aspects of our theory. This is necessarily simplified as well as condensed, so we refer to an interested reader to Papers I, II and III and to Romero-Gómez *et al.* 2009 for more information, a more thorough description of the theory and references to other related work. Nevertheless, the main theoretical concepts and definitions are given so as to make this paper as stand-alone as possible, while avoiding repetition. In particular we introduce here the Lagrangian points, the invariant manifolds and the properties of the associated orbits. Section 3 compares the morphological types of our theoretically predicted density enhancements with the observed ones. Section 4 focuses on the properties of the theoretical and the observed spirals, such as their sense of winding, their number of arms and their pitch angle. Section 5 is devoted to ring properties, such as the frequency of the various types of rings, the axial ratios of inner and of outer rings and the ratio of outer to inner ring major axes. Further comparisons with observations, including pattern speed prediction, the bar shape, kinematics, radial drift and abundance gradients will be discussed in Paper V, the last of this series. There we also give a global discussion of all the results in this series. For this reason we summarise only briefly the results of this paper in Sect. 6.

2 THEORETICAL REMINDERS

Our theory is largely based on the dynamics of the Lagrangian points L_1 and L_2 of a two-dimensional barred galaxy system. These are located along the direction of the bar major axis and are, in the standard case, unstable saddle points (Binney & Tremaine 2008). Each of them is surrounded by a family of periodic orbits, called Lyapunov orbits (Lyapunov 1949). Since these are unstable they can not trap around them quasi-periodic orbits of the same energy¹, so that any orbit in their immediate vicinity (in phase space) will have to escape the neighbourhood of the corresponding Lagrangian point. Not all departure directions are, however, possible. The direction in which the orbit escapes is set by what we call the invariant manifolds. These can be thought of as tubes that guide the motion of particles of the same energy as the manifolds (Gómez *et al.* 2004; Koon *et al.* 2000). Each manifold has four branches emanating from the corresponding Lyapunov orbit, two of them inside corotation (inner branches) and two of them outside it (outer branches). Along two of these branches (one inner and one outer) the mean motion is towards the region of the Lagrangian point (stable manifolds), while along the other two it is away from it (unstable manifolds). We need to stress that the terms ‘stable’ and ‘unstable’ do not mean that the orbits that follow them are stable and unstable, respectively. In fact all the orbits that follow the manifold are chaotic, but they are in a loose way ‘confined’ by the manifolds, so that they stay together, at least for a few bar rotations, in what could be called a bundle. We propose that these manifolds and orbits are the building blocks of the spirals and rings.

These manifolds do not exist for all values of the energy, but only for energies for which the corresponding Lyapunov periodic orbit is unstable. This means energies within a range starting from the energy of the L_1 or L_2 (E_{J,L_1}) and extending over a region whose extent depends on the model (Skokos, Patsis & Athanassoula 2002).

In Papers II and III we classified the manifolds and the corresponding orbits in three categories, the homoclinic, the heteroclinic and the escaping ones. Homoclinic manifolds and orbits start from the vicinity of either the L_1 , or the L_2 and end near the same Lagrangian point. An example is given in the left panel of Fig. 1. Heteroclinic manifolds and orbits start from either near the L_1 , or the L_2 and end near the Lagrangian point located at the other end of the bar, i.e. the L_2 or L_1 , respectively. An example is given in the middle panel of Fig. 1. Finally, escaping orbits start off near one of these Lagrangian points but do not end near either this point or the symmetric one at the other side of the bar. Their name comes from the fact that they escape the vicinity of the bar and reach parts of the galactic disc further out, but this does *not* imply that they escape the system and reach infinity.

The case described so far has five Lagrangian points in total, two unstable and three stable, and is referred to as the standard case. The formation of the manifolds, and therefore of the rings and spirals, depends on the existence of such unstable saddle Lagrangian points as described above. We have, therefore, applied our theory to barred galaxies. It can, however, be applied also to non-barred galaxies with other non-axisymmetric perturbations, provided these have unstable saddle Lagrangian points as described above and in Papers I, II and III. This can include spiral perturbations and will be discussed further in Paper V.

Another alternative, which is interesting both dynamically and morphologically, occurs in barred galaxies when the L_1 and L_2 are stable. This can happen if a sufficiently important amount of mass is sufficiently concentrated around the Lagrangian points, as described in Paper III. In such cases, the L_1 and L_2 become stable, while four other Lagrangian points appear along the direction of the bar major axis, one on either side of the L_1 and L_2 . These new Lagrangian points are unstable and thus work like the L_1 and L_2 in the standard case. The intricacies of the manifolds in such cases have been studied in Paper III, and we will only mention here that the gross global morphology of the system stays roughly unchanged for a wide range of parameter values. Other things, however, such as the axial ratio of the rings can change, as will be discussed in Sect. 5.

In Papers II and III, we calculated manifolds and orbits in three different rigid barred galaxy potentials. Model A is taken from Athanassoula (1992a) and has a Ferrers bar (Ferrers 1877) of semi-major axis a , axial ratio a/b , quadrupole moment Q_m and rotating with a pattern speed Ω_p . The central concentration of this model is characterised by its central density ρ_c . Model D has a Dehnen-like bar potential (Dehnen 2000) characterised by a strength parameter (ϵ) and a scale length (α). The BW model has a Barbanis & Woltjer type potential (Barbanis & Woltjer 1967), characterised by a strength parameter ($\hat{\epsilon}$) and a scale length (r_1). The two latter models have the same axisymmetric part as model A. Ferrers bars have a realistic density distribution, but their non-axisymmetric force beyond corotation decreases strongly with radius. The other two potentials are ad-hoc, i.e. are not associated with a particular density distribution, but can have strong non-axisymmetric forces beyond corotation. As in Papers II and III, we use them to represent forcings not only from bars, but also from spirals, oval discs and tri-axial haloes. A full description of these potentials can be found in

¹ We will all through this paper loosely call ‘energy’ the numerical value of the Hamiltonian in a frame of reference co-rotating with the bar, i.e. a frame in which the bar is at rest, and denote it by E_J .

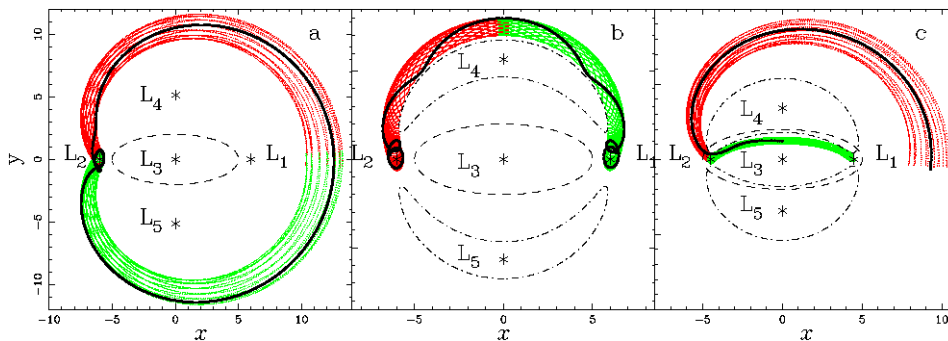


Figure 1. Examples of homoclinic (panel a), heteroclinic (panel b) and escaping (panel c) orbits (black thick lines) in the configuration space. In red lines, we plot the unstable invariant manifolds associated to these orbits, while in green we plot the corresponding stable invariant manifolds. In dashed lines, we give the outline of the bar and, in panels (b) and (c), we plot the zero velocity curves in dot-dashed lines.

Appendix A of Paper III. These bar potentials will be used here together with different types of rotation curves. As in our previous papers, we measure angles in the standard mathematical sense, i.e. starting from the positive x axis and increasing anticlockwise.

As shown in Papers II and III, the properties of the manifolds depend strongly on the relative strength of the non-axisymmetric forcing at and somewhat beyond corotation. We measure this with the help of the quantity Q_{t,L_1} , which is the value of Q_t

$$Q_t(r) = (\partial\Phi(r, \theta)/\partial\theta)_{max}/(r\partial\Phi_0/\partial r), \quad (1)$$

at r_L , the radius of the Lagrangian point L_1 or L_2 , i.e. $Q_{t,L_1} = Q_t(r = r_L)$. This is not the same as the strength of the bar, which is often measured by Q_b , i.e. the maximum of Q_t over all radii shorter than the bar extent. The radius at which this maximum occurs can be small compared to r_L . So Q_b is not necessarily a good proxy for Q_{t,L_1} and vice versa. Nevertheless, for the sake of brevity, we will often replace in our discussions “non-axisymmetric forcings which are relatively strong at and beyond corotation” simply by “strong bars”, or “strong non-axisymmetric forcings”.

3 MORPHOLOGY

Our aim in this work is to show that the dynamics of the manifolds emanating from the unstable Lagrangian points can explain the formation of spirals as well as of inner and outer rings in barred disc galaxies. Thus, in this section, we will make the link between the morphology of theoretical and of observed spirals and rings. At this stage, it is premature to make a detailed comparison for one specific galaxy. Instead, we will make global comparisons and make sure that there are no major differences between models and observations and no obvious discrepancies which would disqualify our theory.

Any candidate theory should reproduce correctly the observed spiral and ring morphologies. Our theory can indeed accomplish this, as we will show in the next subsections. The top two rows of panels of Fig. 2² show four galaxies that contain archetypes examples of the characteristic morphologies that have to be reproduced;

namely spirals, inner rings and the three types of outer rings, R_1 , R_2 and R_1R_2 . They will be described in detail in the following subsections. The upper row of panels gives the images and the second row the schematic plots, bringing out the characteristic morphologies of the galaxies, which the manifolds have to reproduce. The third and fourth rows give manifold examples which reproduce qualitatively the main characteristic features well – the former viewed from an orientation similar to that of the observed galaxy in order to permit a better comparison, the latter viewed face-on.

Note that we have not used the potential of each specific galaxy, nor have we made a search for the best fitting manifold. We simply found, amongst the very large number of models for which we have calculated manifolds, one which roughly represents the desired morphology.

3.1 Spiral structure

The left column of Fig. 2 corresponds to NGC 1365, a galaxy with a strong bar and a clear, well-developed, grand design spiral structure. It has two spiral arms, each emanating from one of the two ends of the bar and extending well into the outer disc. The lower two panels in this column show a model qualitatively reproducing this morphology. It also has two spiral arms, one emanating from each end of the bar and extending outwards. The spiral winding also appears similar and will be discussed in more detail in Sect. 4.3. Thus the model matches qualitatively the morphological properties of the spiral very well.

A further point to note is that in the case of escaping trajectories – i.e. trajectories that wind from L_1 (or L_2) outwards and do not end at the same or the other Lagrangian point – the manifolds become wider as the distance from the centre increases (see e.g. bottom left panel of Fig. 2). Under the assumption that no mass is created or destroyed, this implies that the density in this arm component should decrease with increasing distance from the centre. However, if other arm components – e.g. a weak, leading component – are present, this will lead to bumps on an otherwise smoothly decreasing density profile.

3.2 Inner rings

Inner rings have roughly the same size as the bar (Buta 1986). Buta (1995) studied their orientation with respect to the bar major axis using his catalogue of southern ring galaxies (CSRG). Comparing with model distributions of apparent bar/ring position angles, he

² The images of NGC 1365 (first column, first row) and of ESO 507-16 (third column, first row) are taken from the Digital Sky Survey and those of NGC 2665 (second column, first row) and ESO 325-28 (third column, first row) were reproduced from <http://bama.ua.edu/~rbuta/devatlas> (see also Buta, Corwin & Odewahn 2007). The three schematic plots in the second to fourth column and second row are from Buta & Crocker (1991) and are reproduced by permission of the American Astronomical Society.

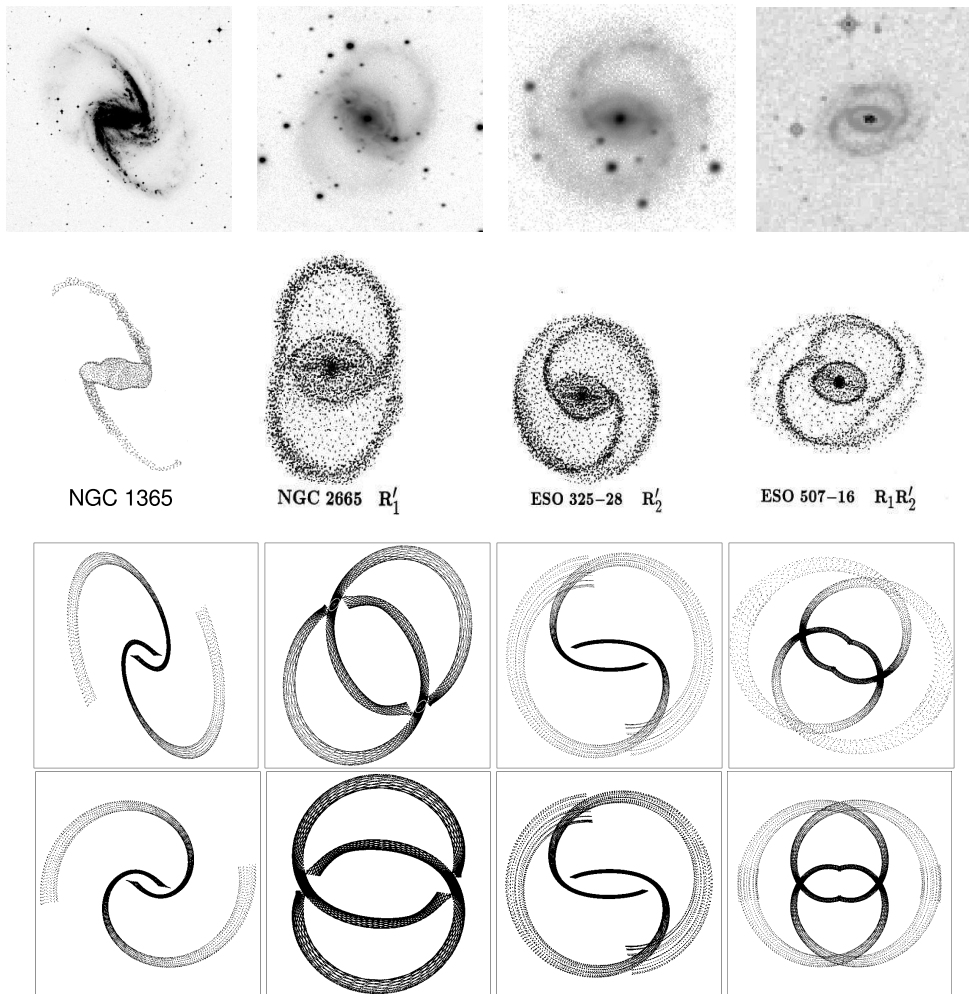


Figure 2. Ring and spiral arm morphologies. The upper row shows four galaxies, typical of the spiral, R_1 , R_2 and $R_1 R_2$ morphologies, namely NGC 1365, NGC 2665, ESO 325-28 and ESO 507-16, respectively. The second row shows schematic plots of these galaxies, bringing out the spiral and ring structures. The third row gives examples from our manifold calculations which have a similar morphology, projected in roughly the same way as the observed galaxy or as the schematic plot. Finally, the fourth row gives the face-on view of these manifolds with the bar along the x axis. Note that, contrary to all other cases, the sense of rotation in the lowest left panel is clockwise in order to ease the comparison with NGC 1365.

found that inner rings are preferentially elongated in the direction of the bar major axis.

In our models, some of the inner manifolds give rise to inner rings while others contribute to the bar, particularly its outer parts. If the L_1 and L_2 are not too strongly unstable, the inner manifolds retrace the same path after one revolution around the galactic centre (Paper III). In this case it is easy to get the outline of the ring. A good example can be seen in the lower two rows of the second column of panels in Fig. 2. Other examples can be found in Papers I, II and III. In these cases, the inner manifold branches outline a ring which has the same morphology as the observed rings. Namely, it has roughly the same extent as the bar and is elongated parallel to the bar major axis. In cases with strongly unstable Lagrangian points, the inner manifold branches retrace the same path only after a few revolutions. Thus the shape of the corresponding density enhancement should be calculated by the self-consistent superposition of the inner manifold loci, and this is well beyond the scope of this paper. To summarise, the inner manifold branches either reproduce well the shape and location of observed inner rings, or populate mainly the outer parts of the bar.

3.3 Outer rings

Outer rings are considerably larger than inner ones, with a major axis of the order of twice the bar size. Depending on the relative orientation of the major axes of the outer ring and of the bar, Buta (1995) distinguished three different types of outer rings. Rings of R_1 type are elongated perpendicular to the bar major axis. Rings of R_2 type are elongated along it and $R_1 R_2$ have a part elongated along the bar and a part elongated perpendicular to it.

NGC 2665, ESO 325-28 and ESO 507-16, shown in Fig. 2 (second to fourth column of the top row), are prime examples of these three types of outer rings. Note that NGC 2665 includes a characteristic feature of R_1 rings. Namely at or near the direction of the bar major axis, the ring approaches the ends of the bar. The features thus formed are called dimples (Buta 1986; Buta & Crocker 1991; Buta 1995) and give to these outer rings a characteristic shape reminiscent of the number 8. Their schematic plots are given in the second row. The third and fourth rows show examples of manifolds with similar morphological characteristics.

The example given in the bottom two rows of the second column reproduces well the characteristic morphology of rR_1 rings in

general and of NGC 2665 in particular. It has both an inner and an outer ring. The latter is elongated perpendicular to the major axis and has the characteristic morphology of a figure ‘8’, with clear dimples near the two ends of the bar. Thus, the manifolds reproduce well all the main observed morphological features of observed rR_1 rings (see also Paper I).

The example in the third column has a different morphological type; that of an R_2 ring. There is a spiral starting from the end of the bar, which, after winding by roughly 90° , joins with an outer ring. The latter is elongated along the direction of the bar major axis, but its ellipticity is rather small, i.e. it is not too far from circular. Also it does not have the dimples seen in the R_1 rings. These morphological characteristics are shared by both the galaxy and the manifold.

The example in the fourth column is of the R_1R_2 morphology and has two outer structures, i.e. two outer rings. The inside one is elongated perpendicular to the bar major axis and has characteristics dimples near the ends of the bar, i.e. it is of the R_1 variety. The outermost one is elongated along the bar major axis, has a relatively small elongation and no dimples in the direction of the bar major axis. All these morphological characteristics are clearly seen in the manifold examples in the last two rows. Also, in all the examples of R_1R_2 morphology we have calculated so far, the R_1 feature lies within the R_2 feature and this also holds for all the observed cases we have seen.

To summarise, we can say that the main morphological features of the three types of outer rings are qualitatively very well reproduced by our theoretical results.

3.4 Bar strength and morphological types

In Paper III we showed that the morphological type – i.e. whether we have a spiral, an R_1 , an R_2 , or an R_1R_2 ring or pseudo-ring – depends on the strength of the non-axisymmetric forcing at the corotation radius. Relatively weak non-axisymmetric forcings give R_1 and R'_1 type morphologies, while stronger forcings give spirals and the remaining types of rings.

A related result was found in Paper II, where we showed that the morphology can also depend on whether the rotation curve is rising, flat or slightly falling in the relevant part of the disc, i.e. at and somewhat beyond the Lagrangian radius. In examples given in Fig. 8 of that paper, we showed that, for the same bar, a rising rotation curve can give a R_1 or R'_1 morphology, while a decreasing rotation will give an R_2 or a spiral morphology. This can now be understood from the results presented in Paper III. Indeed a different axisymmetric model will change the values of Q_t at and beyond the Lagrangian radius, and therefore the morphology and the properties of the rings and spirals. Rising rotation curves imply more mass in the relevant part of the galaxy and therefore a stronger axisymmetric force and a smaller Q_{t,L_1} value, the opposite being true for declining rotation curves. Thus the result found in Paper II is in fact a particular aspect of what was found in Paper III, namely that the morphological type depends on Q_{t,L_1} , the value of Q_t at and somewhat beyond the Lagrangian radius.

This is a clear prediction, which can be tested by observations. In doing so, two points need to be kept in mind. The first one is that the relative importance of the non-axisymmetric forcing depends not only on the bar or spiral, but also on whether the rotation curve is flat, rising or somewhat falling (Paper II). Thus such a test is not possible solely with photometric data, but necessitates also kinematics. The second point to be kept in mind is that a spiral forcing can produce spirals easier than a bar forcing of comparable ampli-

tude. Thus, when comparing spiral to ring morphologies one should keep in mind that the potential of the spiral has to be also taken into account. This has been already argued, albeit in a different context, by Lindblad, Lindblad & Athanassoula (1996).

Making a quantitative comparison is, at this stage, not straightforward because our theory is not self-consistent and because we only use a bar forcing, while in real galaxies the rings and spirals are formed under the combined effect of the bar and of their own potential. The bar forcing is of course much stronger than the spiral one. Buta *et al.* (2005) give for the SB galaxies in their sample for the bar an average Q_B of 0.294 ± 0.21 and for the spiral an average Q_S of 0.171 ± 0.014 . Similarly, Durbala *et al.* (2009), using a sample of isolated barred galaxies of type Sb-Sc, find 0.243 ± 0.015 and 0.166 ± 0.009 for the mean values of Q_B and Q_S , respectively. For the medians they find 0.222 and 0.165, respectively. These numbers can not be directly translated into a ratio of relative effects, because the maximum of the spiral forcing occurs at larger radii than that of the bar forcing. They nevertheless clearly show that the effect of self-consistency will change somewhat the limits between the zones with different morphologies (R_1 , R'_1 , spirals, R_2 , R_1R_2 etc; see Paper III), shifting them to lower bar strengths. The amplitude of this shift will depend on the strength of the spiral, so that no quantitative comparison is possible at this stage.

Buta *et al.* (2005) measured the bar strength for 147 spiral galaxies in the statistically well-defined Ohio State University Bright Galaxy Survey (OSUBGS; Eskridge *et al.* (2000)) sample and found that the average bar strength in barred galaxies with spirals (SB(s) types) is $\langle Q_b \rangle = 0.329$, i.e. higher than the average for all barred galaxies, which is $\langle Q_b \rangle = 0.294$. They also find that the average bar strength in barred galaxies with inner rings (SB(r) types) is $\langle Q_b \rangle = 0.201$, i.e. lower than the average for all barred galaxies. These trends are rough, but still are in good agreement with our theoretical predictions from Paper III.

4 MAIN SPIRAL PROPERTIES

4.1 Why are spirals trailing?

Simply by viewing a spiral galaxy projected on the sky, it is not possible to say whether the arms are trailing or leading, even if one knows the sense of rotation of the material within the galaxy disc. As explained by Binney & Tremaine (2008) and Binney & Merrifield (1998), one needs also to know which side of the galaxy is nearest to us. This can be obtained by studying the obscuration by dust (see e.g. deVaucouleurs 1959 and Sandage 1961 for such pioneering studies). In almost all cases where the result is unambiguous the arms are found to be trailing. In our own Galaxy also the arms are trailing. It is thus generally admitted that spiral arms in disc galaxies are trailing. How does that compare with our theoretical predictions?

The anti-spiral theorem (Lynden-Bell & Ostriker 1967) states that if a steady-state solution of a time-reversible set of equations has the form of a trailing spiral, then there must be an identical solution in the form of a leading spiral. Thus, density wave theory can not distinguish between trailing and leading solutions, unless one takes into account the growth of the spiral.

Swing amplified spirals, however, are not stationary, so do not have this shortcoming (Toomre 1981). The inwards going wave is leading and will be reflected at the centre of the galaxy into an outwards-going trailing wave which will be amplified in the corotation region. Therefore, according to this theory, both a trailing and

a leading component will be present, but since a very strong amplification occurs, the trailing component will have a much larger amplitude than the leading component. Thus, visually one will see a trailing spiral, whose amplitude will present oscillations with radius due to the interaction of the leading and trailing spiral phases (Athanassoula 1984, 1992b; Puerari et al. 2000).

Since the potentials we have used so far are stationary in the rotating frame of reference, the anti-spiral theorem will apply. Indeed, if one reverses the arrow of time in the case of the unstable manifolds – which have a trailing spiral shape – one finds the stable manifolds – which are of the same shape but leading. This is true whenever the bar does not evolve. Material, however, needs initially to get trapped into the manifolds, and this can only be done while the bar is being formed, or while it grows. This introduces time evolution and thus breaks the degeneracy between trailing and leading arms. To understand this further, we made a number of response simulations. For this we considered 10 000 particles initially in circular orbits around the galactic centre and grew gradually (in one bar rotation) a bar in the disc.

Let us start by describing the results of a case which, when the bar has reached its final amplitude, will have a spiral manifold morphology. The response is a trailing spiral which forms gradually while the bar grows. This means that at any time there are more particles in the trailing arm than in the background or the corresponding symmetric leading arm. This, however, does not, on its own, prove that the unstable (trailing) manifolds trap particles as the bar grows, because particles could still traverse the arm, which would then be a density wave.

To reveal the differences between the unstable and stable manifold and to prove that it is mainly the unstable manifold that traps particles, we need to work in phase space rather than configuration space, i.e. we need to consider velocities as well as positions. We thus chose a number of simulation particles at random in the radial range of the spiral arms and in the energy range where the stable and unstable manifolds exist. For each of these, we calculated the manifolds at the particle energy and found the tube they outline in phase space. We then checked whether the particle is trapped by the stable or the unstable manifold, or whether it is not trapped at all. We repeated this for several time steps and a large number of particles and from these results we can get some statistical information. We find that of the order of 30 – 50% of the particles are trapped by the unstable manifold and only 0 – 2% by the stable ones. The remaining particles are either not trapped by any manifold, or it was not possible to give an unambiguous answer due to their locations (e.g. close to the Lagrangian points). This very important numerical difference between the stable and the unstable manifolds shows that our theory can make a strong prediction concerning the sense of winding of the spiral arms. Namely, it predicts that as the bar grows in a galaxy, the unstable manifolds will trap mass elements. Since the unstable manifolds have a winding in the trailing sense, this means that our theory predicts that spiral arms generated by the manifolds of the L_1 and the l_2 Lagrangian points should be trailing, as observed.

The situation is different in the case of a bar which, after the bar has reached its maximum amplitude, has manifolds with the shape of rings. As we already discussed in Paper II, in this case the unstable and stable manifolds connect in phase space, so it is not possible to say whether a particle belongs to the stable or the unstable manifold. Thus, in this case, both stable and unstable manifolds can be populated, so that there is no preference of trailing or of leading windings. This is in good agreement with the observed shape of rings in real galaxies, which have no preferred winding.

Thus to summarise, in the case of spirals, material gets trapped mainly in the manifolds as the bar grows, mainly in the unstable one. This accounts for the preponderance of trailing (as opposed to leading) spirals. In the case of rings, the stable and unstable manifolds communicate in phase space, so there is no preferred sense of winding.

4.2 Number of arms

In the vast majority of cases, spirals in barred galaxies have two spiral arms. This is in good agreement with our theory which relates the spiral arms to the unstable Lagrangian points. In the standard case, a barred galaxy has two unstable Lagrangian points, L_1 and L_2 , which are saddle points (Paper I). Each one accounts for a spiral arm. Thus our standard theory predicts that barred galaxies will have two-armed grand design spirals emanating from a location near one of the two opposite ends of the bar. Since all the forcings we have used so far are bisymmetric, we found by necessity two symmetric spirals. In real galaxies, however, there are always asymmetries in the forcing potential, and this will lead also to asymmetries between the two spirals, or to small angular shifts of their beginning with respect to the tip of the bar. There is thus very good agreement between the results of our theory and observed spirals regarding the number of spiral arms.

Although rare, there are, nevertheless, a few observed barred galaxies with more arms, in particular with a four armed structure (Buta 1995). A good example is ESO 566-24. Can our theory account for such structures?

If more than two Lagrangian points with saddle behaviour were present, our theory could predict spirals of higher multiplicity. The most straightforward way of achieving this is to include a $\cos(m\theta)$ forcing, with $m > 2$ and a sufficiently high amplitude. Making a full analysis of such potentials, of their origin and of the corresponding manifolds is beyond the scope of this paper. We will, nevertheless, examine the iso-effective-potential curves and the type of stability of the corresponding Lagrangian points for some specific cases, in order to get some insight and to test whether such structures are possible. We will also, for simplicity, limit ourselves to $m = 4$ cases, but the extension to other m values is straightforward.

Ferrers bars have eightfold symmetry and forcing terms $m = 2$ and higher. Increasing the bar mass increases both the $m = 2$ and the $m = 4$ terms leaving their ratio unchanged. Increasing the bar ellipticity, however, changes the $m = 4$ over $m = 2$ ratio; thinner bars having larger values of this ratio. In such bars the L_4 and L_5 can become unstable (Athanassoula 1992a), but they become complex unstable, not saddle points. These do have manifolds, both stable and unstable, but it is unclear whether these can account for spiral arms and at a first glance it does not seem very promising. Further theoretical work is necessary to clarify this issue.

The simplest and most straightforward bar potential having the desired properties is of the form

$$\Phi_b(r, \theta) = A_2(r) \cos(2\theta) + A_4(r) \cos(4\theta + \phi(r) + \theta_0),$$

This is bar-like within corotation with only an $m=2$ forcing and spiral-like with $m = 4$ outside it. Fig. 3 shows a specific example, whose iso-effective-potential plot looks promising. Around corotation there are four unstable Lagrangian points of the saddle type, similar to those at L_1 and L_2 in the standard case. At a somewhat larger radius there are four stable Lagrangian points, similar to the L_4 and L_5 in the standard case. Introducing such an m forcing is not the only way to obtain four unstable Lagrangian points with a

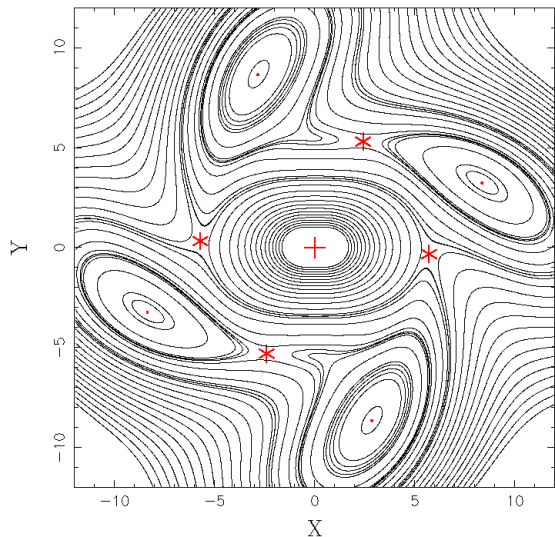


Figure 3. Iso-effective contours for a potential with an $m = 2$ symmetry inside corotation and an $m = 4$ outside it. There are four Lagrangian points in the region around corotation and four more somewhat beyond that. The former are of saddle type and are marked with a red star. The latter are stable and are marked with a red dot. The four-armed barred galaxies, such as ESO 566-24, could be due to potentials of similar type.

saddle point behaviour. This can also be achieved with an $m = 2$ only, provided it has a non-monotonically decreasing profile of the appropriate shape. Again we stress that these are very simple ad hoc potentials, which may not necessarily be linked to a realistic density distribution and do not represent any galaxy in particular. It is nevertheless useful to consider them, because they may give some insight as to what kind of potential can explain the spiral structure in ESO 566-24 (Rautiainen, Salo & Buta 2004), or other, undoubtedly very rare, galaxies of this type.

To summarise, our theory predicts that the vast majority of barred spirals will be two armed, but that, for certain types of potentials, it is possible to have more arms. This is in good agreement with what is indeed found by observations.

4.3 Spiral arm shapes

We showed above that the manifolds have shapes that can reproduce spiral arms. But how does the winding of the manifold loci compare with that of spiral arms in real barred galaxies? To answer this question we deprojected the image of NGC 1365 (upper two panels of the left column of Fig. 2), using viewing angle values obtained by rounding off the estimates given by Jörsäter & van Moorsel (1995), namely a position angle of 220° and an inclination angle of 50° , and we measured at each radius the coordinates of the maxima along the arm. We can now compare the loci outlined by these measurements to the loci of a typical spiral manifold. For this we chose a D model with $\epsilon = 0.05$ and $r_L = 5$. In Fig. 4 we can see that the comparison is very satisfactory. In particular, both observed spirals and calculated manifolds share the common property that after reaching a maximum radius they fall back towards the inner parts of the galaxy. For a more precise comparison we would need to calculate the potential of NGC 1365 from some image in the near infrared as well as kinematics, but this is beyond the scope of this paper.

Thus our theory, explaining the formation of spiral arms in barred galaxies with the help of the invariant manifolds of the L_1

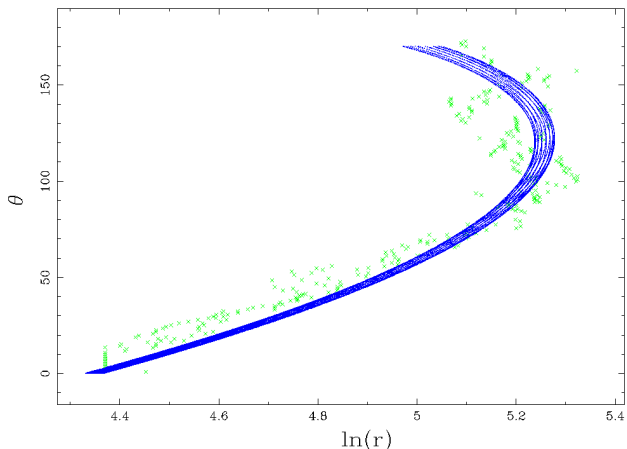


Figure 4. Comparison of the manifold loci on the $\theta = \ln(r)$ plane (blue on the online version, black in the paper version) with the spiral arm loci in NGC 1365 (x signs, green in the online version, gray in the paper version).

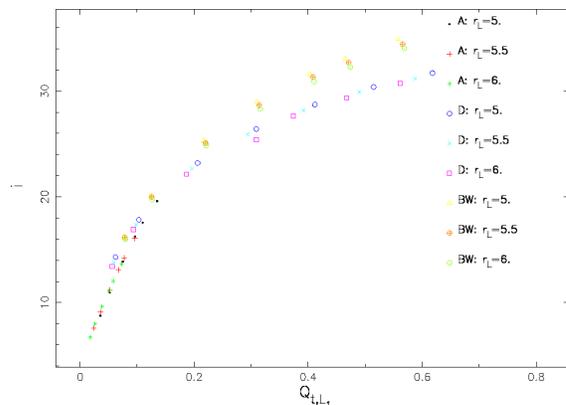


Figure 5. Pitch angle i as a function of bar strength measured by Q_{t,L_1} . We plot the results only for three values of r_L – namely $r_L = 5$, $r_L = 5.5$ and $r_L = 6$ – but we have verified that other realistic values also show the same trend. We include in the plot models from all three families, A, D and BW. For A models we include in the plot only models with a Ferrers’ index $n = 1$, but we verified that models with $n = 0$ lie on the same curve.

and L_2 Lagrangian points, explains the characteristic winding of the spiral arms observed in a large fraction of barred galaxies. Namely, as the angle increases the radius first increases and, upon reaching a maximum radius, ‘falls back’ towards the bar region, or towards the region of the other spiral. This property has not been so far reproduced with density wave models, where the spiral arms tighten up as they reach outer Lindblad resonance, but do not fall back (Lin, Yuan & Shu 1969 and later works of this group, Athanassoula 1980 for an approach not relying on the WKBJ approximation).

4.4 Trends with the pitch angle

In order to assess how various bar parameters affect the winding of the spiral, we obtained the value of the pitch angle by fitting a logarithmic spiral

$$\theta - \theta_0 = \cot i \ln(r/r_0)$$

over the main relevant part of the manifold, for many models. We examined each of our three model families separately (families A,

D and BW), and used as a measure of the bar strength Q_m , ϵ and $\hat{\epsilon}$, respectively. We find that (not shown here), for all three families, the pitch angle increases with increasing bar strength and the form of the dependence is similar. In other words, the spirals corresponding to stronger bars are more open than those from weaker bars. This is a direct consequence of the spiral properties described in section 3 of Paper III. To our knowledge, no such relation has as yet been reported by observations. It would be thus very useful to test whether such a relationship can indeed be found. In order for this to be possible, we need first to check whether the trend persists when the pitch angle of the various models is plotted as a function of a common bar strength measure. For the latter we use Q_{t,L_1} and show the results in Fig. 5 for the three model families and three pattern speed values. The trend is clearly present, with relatively little spread due to the different models. The pitch angle increases steeply as Q_{t,L_1} increases from 0 to 0.2, and has a more shallow increase beyond that. It is not easy to confront this result with measurements from the barred galaxies of the OSU and the Frei samples (Eskridge *et al.* 2000; Frei *et al.* 1996) for mainly two reasons. The first difficulty lies in the deprojection of the galaxies, since the value of the position and inclination angles can be heavily influenced by the outer parts of the arms. This is the well known Stock's effect (Stock 1955) and may influence tightly wound spirals differently from open ones. This could introduce a bias in the analysis and thus has to be treated with particular care. The second difficulty comes from the fact that the quantity Q_{t,L_1} is not easy to obtain from observations since it implies knowledge of the corotation radius and some information of the dark matter content in this region.

Such a relation has not been found by density wave theory because this has been fully developed only in the linear regime, so that a change in the bar amplitude will only change the amplitude of the spiral (for reviews, see Toomre 1977 and Athanassoula 1984). It is, however, present in the response simulations of Schwarz (1984), as expected, since, as we showed in Paper III the gas-response spirals and rings obey manifold dynamics.

5 MAIN RING PROPERTIES

5.1 Frequency of ring types

Buta (1995) classified 3692 galaxies in his CSRG catalogue and found that about 53% of them have an outer ring, 25% of the galaxies with an outer ring have an R_1 ring or R'_1 pseudo-ring morphology. About 15% have an R_2 ring or R'_2 pseudo-ring and 4% an R_1R_2 ring morphology. The rest of the ringed galaxies have a single near circular outer ring.

Our model reveals what part of the parameter space corresponds to what type of rings (see Paper III), but we can not translate this into frequencies of observed ring types because our models are not exact replicas of observed bars. It is possible, however, to make a few relevant comments. In particular, in Fig. 4 of Paper III we examined the morphology of models with Ferrers bars, which are, to date, the most realistic analytic bar model potential. For these, we found that in most cases the manifold morphology is of R_1 , or R'_1 type. This is in good agreement with the fact that R_1 is the most frequently observed of the three ring types. Although this agreement is very welcome, it should not be considered as a confirmation of our theory. On the other hand, it would have been worrying if observations showed that R_2 , or R_1R_2 rings were most common since this would have implied a rather bizarre distribution of bars on the (bar

strength, bar pattern speed) plane, and/or very strong differences between Ferrers potentials and the potentials of observed bars.

5.2 Ratio of ring sizes

5.2.1 General remarks

As shown in Paper III, ring sizes depend strongly on the model potential used. Moreover, our models are not exact representations of observed bars and we neglect the self-gravity of the ring structure. Therefore, quantitative comparisons of model and observed ring ratios may well not show agreement.

There is a further complication concerning the measurement of inner ring sizes in models. As described in Paper III, weak bars have weakly unstable L_1 and L_2 Lagrangian points and, after a revolution around the galactic centre, the inner manifold branches retrace the same path, thus forming the inner ring. In these cases it is relatively easy to measure the length of the major and minor ring diameters. On the other hand, strong bars have strongly unstable L_1 and L_2 and the inner manifold branches cover a new path after the first revolution around the galactic centre, retracing the same loci only after a couple or a few revolutions (Papers III and V). One of these loci could correspond to the ring, and the others to the outer parts of the bar, or all could correspond to the bar. In the latter case there will be no inner ring, while in the former one it is not easy to find the ring outline. In principle, this should be measured from the self-consistent superposition of the corresponding manifold parts. This, however, is beyond the scope of this paper, so in what follows we measured, whenever relevant, the size and shape of the inner ring from the loci of the *first* revolution of the inner manifold branches. This is arbitrary and thus could lead to considerable systematic errors. In particular, it could lead to a considerable underestimate of the ring minor axis. This will be discussed further below.

Further reasons for discrepancies can stem from the observations. Galaxies are observed as projected on the sky, i.e. are not necessarily face-on, and thus the axial ratios can not be directly compared to models. Buta (1995) gave statistical estimates of the deprojected axial ratios from a careful analysis using a model and relying on assumptions. The obvious and indisputable assumption is that the observed galaxies are oriented randomly with respect to the line of sight. Nevertheless, since rings can not be seen in edge-on, or near edge-on, discs, there is a bias against highly inclined cases, which is dealt with in the modelling by an approximation. Further assumptions include the fact that both discs and bars are vertically infinitesimally thin, that the ring shapes are well approximated by ellipses, and that the intrinsic shape of the axial ratio distribution is either top-hat with a narrow extent (Buta 1986), or Gaussian (Buta 1995). Moreover, problems may also come from selection effects in the catalogue, especially for rings with small diameters. Thus, the errors stemming from observations can also be important. They will, moreover, be more severe for inner than for outer rings and will bring an artificial reducing of the number of small axial ratio cases (Buta 1995).

Despite the above arguments, we attempt in this section not only qualitative but also quantitative comparisons and estimates, but it should be kept in mind that the latter may be affected by non-negligible error, particularly in the case of inner rings. Let us call D_o and d_o the lengths of the major and minor axes, respectively, of the outer ring and by D_i and d_i the same quantities for the inner ring. The relevant quantities which we can use to make comparisons with observations are d_o/D_o , d_i/D_i and D_o/D_i .

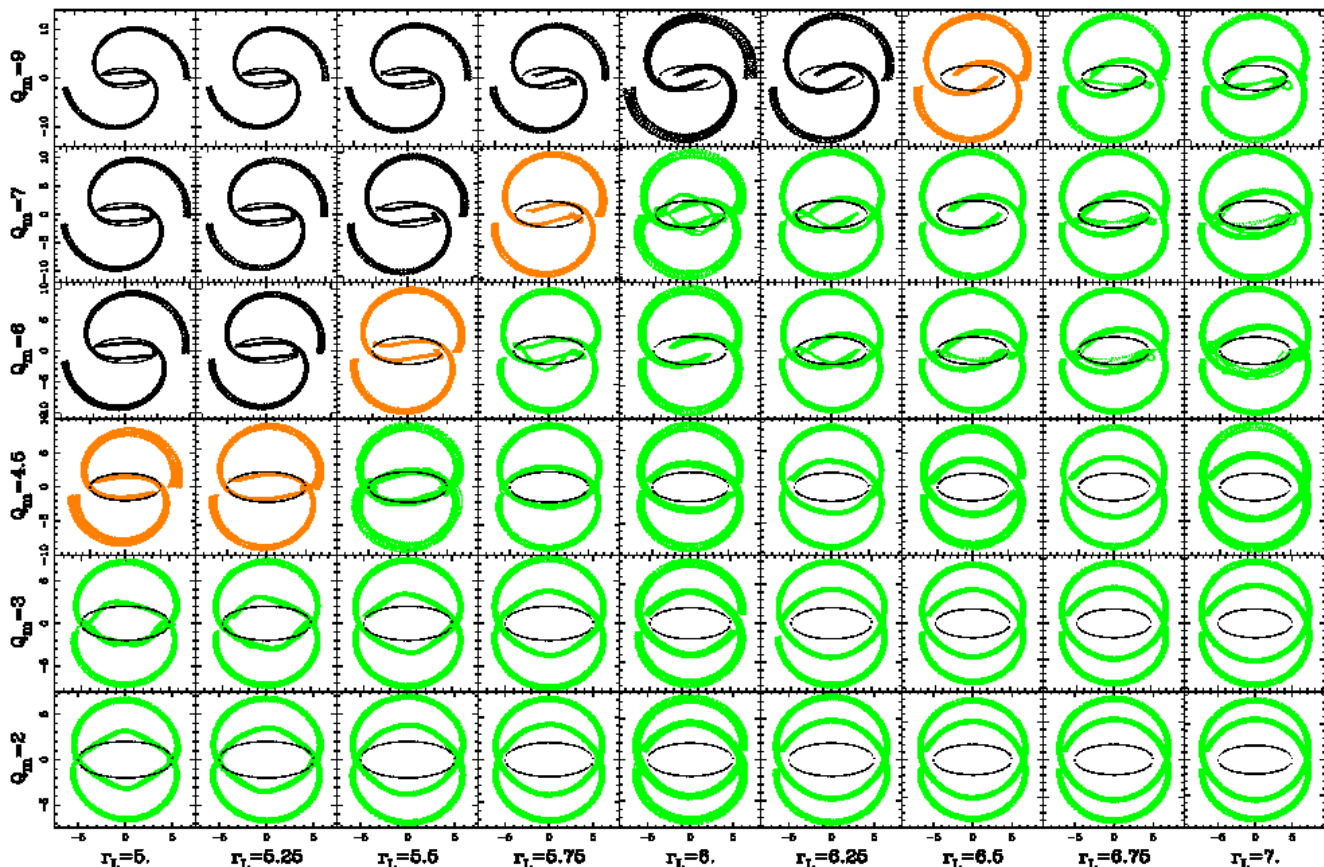


Figure 6. Effect of the bar strength and of the Lagrangian radius r_L on the manifold loci for a model with a Ferrers bar and a slightly decreasing rotation curve (see text). The strength of the bar is parametrised by the quadrupole moment Q_m . Each panel corresponds to a pair of (Q_m, r_L) values, given on the left (in units of 10^4) and on the bottom of the figure, respectively. The manifolds are plotted in a colour which is determined by their morphology: green for R_1 , orange for R'_1 and black for spirals. The thin, black lines give the outline of the bar. Compared to fig. 4 of Paper III, which has an identical bar model, this plot shows how a change in the axisymmetric component can affect the morphology of the response and the axis ratios of the rings.

Table 1. Results for models with lenses: Axial ratio of the inner and outer ring sizes (d_i/D_i and d_o/D_o , respectively) and Q_{t,L_1} as a function of the relative lens mass, f_{lens} (see text for more information).

f_{lens}	1			2		
	Q_{t,L_1}	d_i/D_i	d_o/D_o	Q_{t,L_1}	d_i/D_i	d_o/D_o
0.	0.077	0.51	0.76	0.077	0.51	0.76
0.2	0.079	0.57	0.80	0.087	0.53	0.75
0.5	0.062	0.67	0.81	0.076	0.55	0.75
1.	0.045	0.75	0.86	0.063	0.61	0.77

5.2.2 Further models

Since the ring shapes and the ratio of ring major axes diameters may depend crucially on the adopted potential, we will, in the next few subsections, consider not only models A, D and BW (see Paper III), but also other potentials.

To model galaxies with lenses, we add an extra Ferrers component which corotates with the bar and has the same major axis as it (Kormendy 1979). The remaining parameters were taken as for the fiducial model of Paper III, i.e. $a = 5$, $a/b = 2.5$, $r_l = 6$, $Q_m = 4.5 \times 10^4$, $\rho_c = 2.4 \times 10^4$ and $n = 1$, all measured in the units given in Appendix A of that paper. The lens has an axial

Table 2. Results for models with unstable or stable L_1 and L_2 Lagrangian points: Axial ratio of the inner and outer ring and stability of the L_1 and L_2 as a function of the relative stabilising mass F (see text and Paper III for more information on the models).

F	stability	d_i/D_i	d_o/D_o	D_o/D_i
0.	unstable	0.81	0.90	1.50
0.19	unstable	0.70	0.92	1.60
0.20	unstable	0.72	0.91	1.71
0.29	stable	0.64	0.85	1.91
0.41	stable	0.60	0.85	2.06
0.49	stable	0.55	0.84	2.07

ratio $b/a = 0.9$ and a mass $M_{lens} = f_{lens}M_b$, where M_b is the mass of the bar. The results are given Table 1 for two such series of models. In the first one the total mass of the model was kept constant (columns two to four, marked 1), so that a certain fraction of the bar mass was converted into a lens. For the second one the lens was simply added on to the model, without any change of the bar mass (columns five to seven, marked 2). For the first series, increasing the lens fraction decreases Q_{t,L_1} (as expected), and renders the inner and outer rings more axisymmetric. For the second series of models, adding a lens makes a less clear-cut effect, because the total mass of the model does not stay constant. It is, however, clear

that it makes the inner ring more axisymmetric and does not have a big effect on the shape of the outer ring.

We also considered models in which the L_1 and L_2 Lagrangian points are stable. As in Paper III, this stability was achieved by adding two mass concentrations in the form of Kuz'min/Toomre discs (Kuz'min 1956; Toomre 1963) each centred on one of the L_1 and L_2 Lagrangian points. In the examples given here we adopted for these discs a scale-length $r_a = 0.6$ and we tried several values of the fractional mass F , where $F = M_{KT}(r < r_a)/M_b(r < r_a)$ is the ratio of the mass of one of the Kuz'min/Toomre disc (M_{KT}) to that of the bar (M_b), both calculated within a radius equal to r_a from their respective centres (see Sect. 5 in Paper III for more information). These values, the resulting stability and the measured outer ring axial ratios are listed in Table 2. We note that, as F increases past a certain threshold, the L_1 and L_2 turn from unstable to stable. An increase in F makes the inner ring considerably more elongated, and has a smaller effect on the outer ring axial ratios, which furthermore is not always monotonic. As a result, the ratio of outer to inner major axes increases considerably with F .

We also analysed the results for two further models, similar to model A but with a different axisymmetric component. For the first one we chose the axisymmetric potential leading to the circular velocity curve denoted by D in Paper II (see Fig. 7 in that paper.). This is slightly decreasing in the regions around corotation and immediately beyond it. Thus, Q_{t,L_1} will be somewhat larger than for model A. We used the same bar model and calculated the manifolds for the same grid of parameter values as for model A in Paper III. We call this model AD and give the corresponding manifold morphologies in Fig. 6. Some notable differences are clear (compare Fig. 6 of this paper with fig. 4 of Paper III), the most important one being that there are many more spirals here than for the previously used rotation curve. This is in agreement with the results and discussions made so far, since higher Q_{t,L_1} values lead to spiral morphologies and lower ones to an rR_1 morphology (Paper III and Sect 3.4 of the present paper).

We also tried another axisymmetric component, such that the peak of the circular velocity curve is nearer to the galactic centre, i.e. more adequate for early type galaxies, and we denote the corresponding model by AE. This introduced relatively little change to the ring shapes, as will be discussed in the following sections.

5.2.3 Outer ring axial ratios

Analysing the results from his CSRG catalogue, Buta (1995) finds that the outer rings have a significantly oval intrinsic shape, with an average intrinsic axial ratio of $\langle q_o \rangle = 0.87 \pm 0.14$. For his SB sub-sample alone, he finds $\langle q_o \rangle = 0.82 \pm 0.07$. He also finds that the outer rings are rounder in SA than in SB galaxies, with an average intrinsic axial ratio of 0.97 ± 0.21 . Applying the same procedure to the Southern Galaxy Catalogue (SGC) he finds $\langle q_o \rangle = 0.83 \pm 0.01$ (Buta 1995), while in a previous study with a somewhat different procedure he finds that the preferred axial ratio range is 0.7 – 1 for SB galaxies and 0.8 – 1 for SAs and SBAs (Buta 1986). There is thus general agreement between the various estimates of the observed outer ring shapes.

Amongst the roughly 300 models discussed in Sect. 3 of Paper III and in Sect. 5.2.2 above, 180 have an R_1 or R'_1 morphology. This number is sufficiently large for us to be able to make some analysis. We therefore measured the major and minor axes of the outer ring for this sub-sample and plot their ratio as a function of Q_{t,L_1} in Fig. 7. We have too few R_2 models for any reasonable

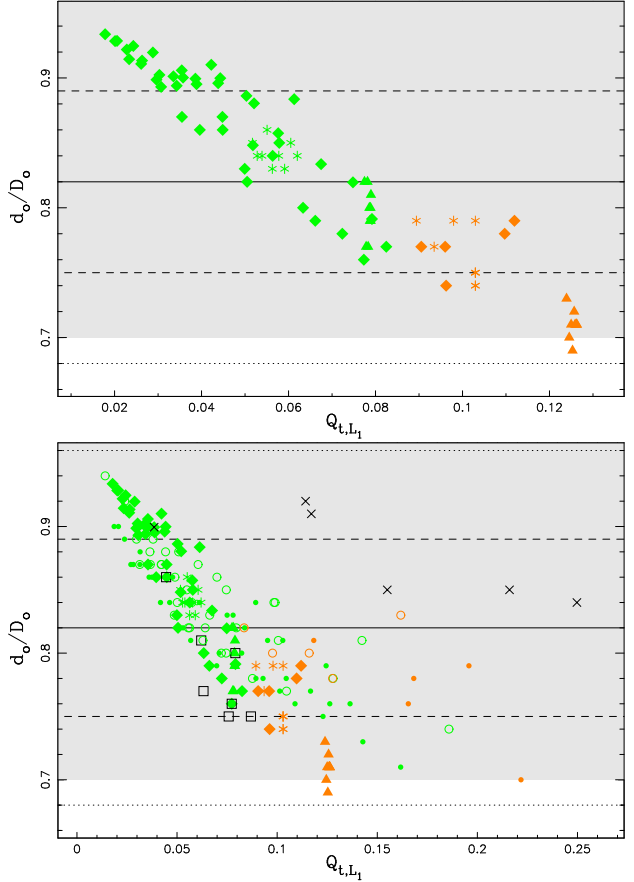


Figure 7. Relation between the strength of the bar in the corotation region, measured by Q_{t,L_1} , and the axial ratio of the outer R_1 , or R'_1 ring for our models. As in Paper III, different colours stand for different morphologies: green for R_1 and orange for R'_1 . The upper panel includes only morphologies for models A, D and BW and shows a strong correlation, in the sense that galaxies with stronger bars have also more elongated outer rings. Results from models A are given by filled diamonds, from models D by asterisks and from models BW by filled triangles. In the lower panel we add more models. Models AD are plotted with a filled circle and models AE with an open one. Models with lenses are plotted with an open square and models from Table 2 with an x sign. The horizontal lines give statistical information on the observed outer ring axial ratios, namely the mean (solid line) as well as the one σ (dashed) and the two σ (dotted) deviations from it, as calculated for barred galaxies from the CSRG (Buta 1995). The grey area shows the region of values found from the SCG survey (Buta 1986). Note that the outer ring axial ratio values we find from our models are in the right range.

analysis and this morphology is also more rare in real barred galaxies. Finally we can not compare the properties of R_1R_2 rings with observation, because the measurements are not uniquely defined since it is not clear whether one should measure the R_1 , or the R_2 part. Buta (1995) measures both and then takes an average of the values weighted according to the strength of each feature. We can not do this for our models because the manifold calculations we presented so far can give us information on the existence and shape of a feature, but not on how much material is trapped by it, the latter depending on the evolutionary history of the galaxy. We thus have no information on how strong the R_1 and R_2 are. In order to obtain this information, we would need to follow the trapping by the manifold during the disc formation and evolution stage. A simplified version of such a calculation has been given in Sect. 4.1, but

a more realistic version would necessitate considerable knowledge on how the disc and its main substructures were formed.

The horizontal lines in Fig. 7 give the average value and the one and two sigma deviations from it for barred galaxies from the CSRG (Buta 1995). The grey area shows the region of values found from the SCG survey (Buta 1986). We note that the values we find from our models are in the right ballpark. In fact, all values are within two sigma from the observed mean and most models are within one sigma from it. Adding results from other types of models (with different axisymmetric components, or lenses, or stable L_1 and L_2 Lagrangian points – see Sect. 5.2.2) does not change in any qualitative way these results (lower panel of Fig. 7). Concerning the outer ring shape, there is thus very good agreement between theory and observations, which holds for all the very wide range of potentials we used.

The upper panel of Fig. 7 shows a tight correlation, in the sense that galaxies with stronger bars have also more elongated outer rings. Most of the points on this plot correspond to A models, with some D and BW models. In fact, it would have been rather difficult to assert the existence of this correlation from the D or from the BW models separately, because their Q_{t,L_1} values are rather clustered. Nevertheless, both the D and BW models fall well on the correlation outlined by the A models, thus reinforcing it.

Let us now check whether this correlation still holds for a yet wider set of model potentials (lower panel of Fig. 7), namely all those introduced in Sect. 5.2.2. All models with lenses fall neatly on the correlation. Most of models with a AD or AE axisymmetric component fall also on or very near the correlation. Only four points (out of 180) are considerably off. Furthermore, three of these correspond to marginal cases, i.e. cases which could be classified either as R'_1 , or as spiral. Thus we can conclude that, although the correlation is widened and could be called a trend, it is certainly still present, even with the very wide variety of the models used. This figure also gives an indication that, for this trend at least, the axisymmetric part of the potential, i.e. the circular velocity curve, makes more difference than the analytical expression used for the bar potential. Considerable more work is, however, necessary in order to assess this.

On the other hand, models with stable L_1 and L_2 Lagrangian points definitely stand apart from the rest and are off the correlation although they have realistic values of the outer ring axial ratio. It is unclear at this point whether this argues only that this correlation will not be followed by models with stable L_1 and L_2 Lagrangian points, or, more strongly, that the correlation will be followed only by certain types of model potentials.

It would be interesting to check whether the correlation we find in Fig. 7 is also valid for *observed* R_1 and R'_1 outer rings. It is in agreement with the average values found by Buta (1995), since these show that barred galaxies have more elongated outer rings than non-barred ones. Unfortunately, it is not possible to make any more accurate tests with only the CSRG data, because it is necessary to deproject each galaxy individually before measuring the ring axial ratios. Furthermore, it is necessary to use an appropriate measure of the bar strength. The correlation in Fig. 7 uses Q_{t,L_1} which measures the non-axisymmetric forcing at corotation. Any such measure at this radius, or somewhat beyond should be appropriate. Measures at smaller radii, however, may not be. To check this further, we replotted the data of the lower panel of Fig. 7, now using Q_b as a bar strength measure. This quantity is very often used in both theoretical and observational studies (e.g. Buta, Block & Knapen 2003; Buta, Laurikainen & Salo 2004; Laurikainen, Salo & Buta 2004;

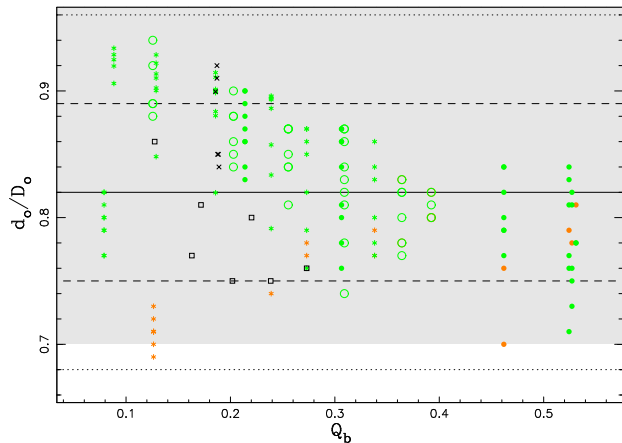


Figure 8. Outer ring axial ratio as a function of the bar strength. The latter is measured by Q_b (see text for definition). Models A, D and BW are plotted by asterisks. The remaining symbols, and the colours, lines and shading are as in the lower panel of Fig. 7.

Laurikainen et al 2004; Durbala et al 2009 and references therein). It relates to the maximum non-axisymmetric forcing and is defined as the maximum of $Q_t(r)$ in the bar region.

The result is shown in Fig. 8. We have not included the results from the Dehnen models, because this ad hoc potential makes it difficult to measure Q_b for the parameters we are using. Even without these points, however, there is no clear correlation. The best correlation is obtained if we look at models A alone and exclude all others. For this case, the rank correlation coefficient is -0.81, while the same models when plotted as a function of Q_{t,L_1} give a rank correlation coefficient of -0.94. Thus the correlation is less tight, but the trend itself is not lost. On the other hand, if we include also the BW models, then the rank correlation coefficient becomes -0.001 for Q_b and -0.95 for Q_{t,L_1} , so that the correlation is quite strong for Q_{t,L_1} and is totally lost for Q_b . Thus, whether it is possible to use Q_b instead of Q_{t,L_1} depends on the comparison at hand. In general, for properties related to the bar or to the inner manifolds Q_b should be a good quantity to use. For the properties of the spirals and outer rings, however, the use of Q_b may be hazardous. In the absence of any further information it is safer and preferable to avoid the use of Q_b for comparison with observations related to the spirals and rings. Nevertheless, Q_{t,L_1} is a more difficult quantity to obtain from observations than Q_b , since it presumes an albeit rough knowledge of the Lagrangian radius r_L . In Paper V we discuss how this quantity can be obtained with the help of our theory and how reliable this estimate can be in various cases. One can thus conclude that such comparisons with observations should be done with great care since the value of Q_{t,L_1} may contain some error due to a wrong estimate of r_L , while Q_b may give wrong estimate of Q_{t,L_1} and therefore of the quantities that depend on it.

5.2.4 Inner ring axial ratios

Buta (1995) analysed the inner ring data from the CSRG in a similar way as for the outer rings. He finds that the inner rings have a significantly oval intrinsic shape and in fact are on average more elongated than outer rings. For his SB sub-sample he finds $\langle q_o \rangle = 0.81 \pm 0.06$, where $\langle q_o \rangle$ is the average intrinsic axial ratio. As discussed above for outer rings, he can not seek correlations of the ring axial ratio with galaxy, or bar parameters because this would necessarily imply deprojecting each galaxy individually.

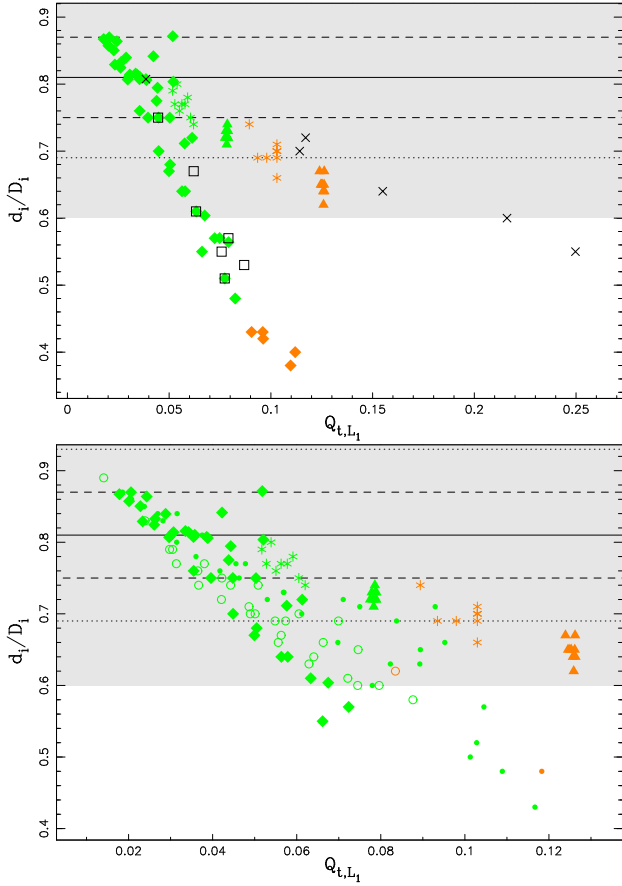


Figure 9. Relation between the strength of the bar near corotation, measured by Q_{t,L_1} , and the axial ratio of the inner ring for our models. There is a strong correlation, in the sense that galaxies with stronger bars have also more elongated inner rings. The horizontal lines and the gray areas give some statistical information on the corresponding observed quantities (see text). Colours and symbols are as in Fig. 7, upper and lower panels, respectively.

He does, however, find that inner rings are rounder in SA than in SB galaxies with an average intrinsic axial ratio of 0.92 ± 0.09 for the former. Applying the same procedure to the SGC, Buta (1995) finds $\langle q_o \rangle = 0.82 \pm 0.02$, while in a previous study with a somewhat different procedure Buta (1986) finds that the axial ratios are uniformly spread in the range 0.60 – 0.95 for SB galaxies and 0.85 – 1 for SAs.

Fig. 9 gives the same information as Fig. 7, but now for inner rings. Results from model A (upper panel) show a very tight correlation between the inner ring axial ratio and the Q_{t,L_1} measure of the bar strength. Models with lenses also lie on the same correlation. Models D and BW (upper panel) also show a correlation, which is followed by the models from Table 2. The regression lines of these two correlations, however, do not coincide, the former being much steeper than the latter.

A further point which is clear from the upper panel of Fig. 9 is that some of the models have an inner ring shape which is much more elongated than the observations. Several arguments need to be taken into account here. It should be kept in mind that all the biases, both observational and theoretical, tend, as discussed in Sect. 5.2.1, to increase this discrepancy and their cumulated effect could be considerable. Amongst the most important ones is the fact that, as we already mentioned, the inner manifold branches can correspond

either to the ring or to the outer parts of the bar. For models A, AD and AE where the bar outline is known, it is possible to distinguish between the two. Unfortunately this is impossible for models D and BW and not straightforward for models from Table 1 or Table 2. We examined all our A, AD and AE models and eliminated those for which the inner manifolds are more likely to correspond to the bar than to an inner ring. This exercise is not trivial, because our calculations are not self-consistent, i.e. the gravity from the manifold itself is not taken into account. If the manifold locus is somewhat outside, but near the bar outline, then in real galaxies, or in self-consistent calculations, the bar outline could somewhat change due to the gravitational pull from the manifold and, provided the distance between the two is small, the two could merge. This is something we can not take into account with our calculations. We thus eliminated only the cases where we estimated from our non-self-consistent simulations that the manifold pertained to the bar more than to the inner ring. We then plot the remaining models, including all possible families, in the lower panel of Fig. 9.

Note that most of the models are in the area outlined by the observations, but a handful are still clearly outside. We examined by eye these cases and found that they are borderline, i.e. perhaps a self-consistent calculation would lead us to classify them as contributing to the outer part of the bar, rather than to the ring.

We also examined which potentials increase this discrepancy, i.e. make more elongated inner rings, and which alleviate it. First considering the rotation curves, we see that AD rotation curves create more elongated rings, i.e. increase the discrepancy between models and observations. This can be understood since in AD models the axisymmetric force is relatively smaller over some of the relevant radial extent than in A models and this, according to our previous results, should lead to more elongated rings, as is indeed found. For models AE the difference is less clear-cut. We can, however, see that for the largest Q_{t,L_1} values, the AE have less elongated rings than the A models, thus alleviating the discrepancy. This can be understood by the fact that, for the most elongated rings, the inner manifold branches reach radial regions where the axisymmetric force is relatively smaller in the AE models than in the A ones. This would then lead to less elongated inner rings in the cases with largest Q_{t,L_1} , as indeed found in our calculations.

The problem of too elongated inner rings was already encountered by Schwarz (1985), who attributed it to the potential he was using. To solve it he proposed to include a lens component. Fig. 9 and Table 1 show that this is indeed a possible solution. For example, the inner ring axial ratio of one of the A models, which without a lens is equal to 0.51 (i.e. nearly three sigma below the average), becomes 0.75 (i.e. within one sigma from the mean) if half of the bar mass is turned into a lens. This of course can not be the only solution, since not all galaxies with inner rings have lenses.

The above argue convincingly that the axial ratio of the inner ring depends on the potential used, stronger relative non-axisymmetric forcings leading to more elongated rings. The results we get with our potentials are in relatively good agreement with observations and an excellent agreement could be reached if the non-axisymmetric forcings in the models were somewhat lower in the region covered by the inner ring.

5.2.5 Statistics on the major axis ratios

Analysis of the ratio of outer to inner ring sizes in observed galaxies has shown that the corresponding histogram is rather concentrated to values around 2 (Athanassoula et al. 1982; Buta 1986, 1995). This is a clear-cut result and it would be nice to test our models

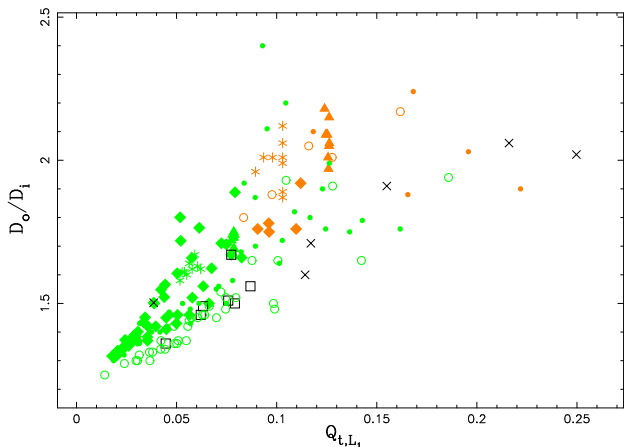


Figure 10. Ratio of the major axis of the outer ring to the major axis of the inner ring as a function of Q_{t,L_1} for all our models. Green symbols denote measurements from R_1 models, and orange ones from R'_1 models. The symbol used depends on the model potential. Results from models A are given by diamonds, from models D by asterisks and from models BW by filled triangles. Models AD are plotted with a filled circle and models AE with an open one. Models with lenses are plotted with an open square and models from Table 2 with an x sign.

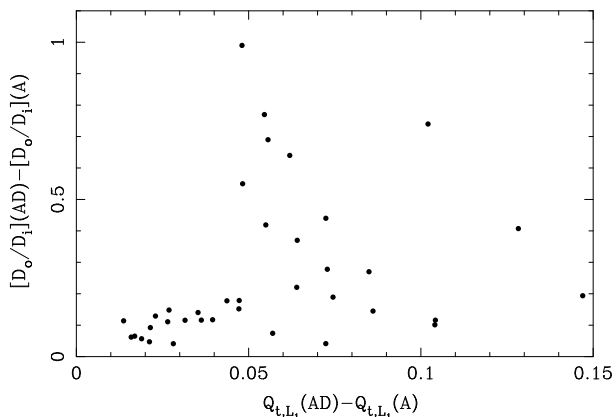


Figure 11. The effect of a change of the model circular velocity curves on the ratio of the outer to inner major axes. The bar parameters do not change, so that each point shows the difference between two models with the same bar, but different circular velocity curves. On the abscissa we plot the difference between Q_{t,L_1} for model AD and the same quantity for model A. On the ordinate we plot the difference between the ratio of the outer to inner major axes, D_o/D_i , for models AD and the same quantity for model A. We note that the change from A to AD increases both the value of Q_{t,L_1} and of D_o/D_i , thus bringing the latter measurements nearer to the observed values.

with it. However, as already discussed in detail in Sect. 5.2.1, this is a very difficult comparison to make, since the ratio in question is strongly affected by errors and biases due to both difficulties in measuring the observed and the model ring sizes and to the fact that measurements in observations have not been done in individually deprojected galaxies. Finally, it should be remembered that we can compare the range of values covered by observations, but we can not compare the corresponding distributions, since the models we have presumably do not cover the parameter space in the same way as the observed galaxies. In fact the observed distribution of some of the relevant parameters is still largely unknown, although considerable progress has been made for others (Gadotti 2009). We will,

nevertheless, attempt a general discussion and comparison with observations and try and outline which types of potentials give the best (or the worst) results.

Fig. 10 shows the ratio of the outer to inner ring major axes, D_o/D_i , plotted as a function of Q_{t,L_1} . It is clear that although a large number of our models have values in the same ballpark as the observations, many have considerably smaller values. Fig. 10 also shows a trend which, although it is not sufficiently tight to be called a correlation, is still very clear. Namely, the ratio D_o/D_i is smaller in cases with smaller Q_{t,L_1} values. Fig. 10 also gives valuable information on which types of potentials are in better agreement with the observations.

All models with an R'_1 morphology have a ring ratio in agreement with observations, independent of the type of potential used. The same is true for nearly all models of the AD type, as well as for models whose L_1 and L_2 Lagrangian points are stable. All these give results which are roughly in the right range of values. On the other hand, many of the remaining cases give smaller values of the axial ratio, i.e. outside the desired region. Such results come from models with an rR_1 morphology with potentials A, or AE.

To make the effect of the circular velocity curve clearer we compare in Fig. 11 models A to models AD. For this we consider pairs of models having the same bar parameters, but one having an A circular velocity curve and the other an AE one, and calculate the difference in Q_{t,L_1} and in the ratio of outer to inner ring major axes, D_o/D_i . We see that both quantities are larger for AD models and that the difference can be considerable. Thus such a change would bring our D_o/D_i in better agreement with observations.

This clearly underlines the effect of the properties of the model potentials on quantitative measures and fully justifies the corresponding arguments advanced in Sect. 5.2.1. It should *not*, however, be interpreted as arguing that rotation curves should be slightly decreasing at and beyond corotation. It argues instead for somewhat larger Q_{t,L_1} values in that region, something that could be also due to a somewhat larger non-axisymmetric forcing. This would be the case in self-consistent treatments, since the potential from the non-axisymmetric rings would be included, and also if the bar model potential dropped less abruptly with radius than the $n = 1$ Ferrers models we use. Thus, such an increase seems very natural and it would easily lead to values of the ring size ratios in good agreement with observations.

6 SUMMARY

In previous papers (Papers I, II and III) we proposed a theory to explain the formation and properties of rings and spirals in barred galaxies. In this paper we compared their morphological properties to that of observed ones. Our theory can produce both spirals and inner and outer rings. Furthermore we get all three observed types of outer rings, i.e. R_1 , R_2 and R_1R_2 rings and pseudo-rings, and no other morphologies. This means that all outer rings produced by our theory have a qualitatively realistic morphology and that all observed morphologies are qualitatively reproduced. We also reproduce the dimples often seen clearly in R_1 rings. Furthermore, we predict that if the non-axisymmetric forcing is relatively low the resulting morphology will be an R_1 ring, while if it is stronger, it will be a spiral.

Spirals due to this theory start off from a location not far from the end of the bar and are trailing, in good agreement with observations. They are in the vast majority of cases two armed, although it is possible, if specific potentials are used, to have arms of higher

multiplicities. Their shape is also realistic and we made a successful quantitative comparison with the arms of NGC 1365. They are able to reproduce the “fall back” of the arm towards the more inner region, seen in NGC 1365 and in many other barred spirals, something which density wave theory could not achieve. We also predict that stronger non-axisymmetric forces in the region around and somewhat beyond corotation will result in more open spirals.

Quantitative comparisons are less straightforward to make, not because they imply tighter constraints, which they do not, but because they involve not only the theory, but also the potential to which it is applied. We are confident that our theory is dynamically correct, and the comparisons with observations made here and in Paper V make us optimistic about its applicability to galaxies with spirals or rings. On the other hand, we are aware of the shortcomings of our potentials. First and foremost, our analysis is not self-consistent, so that we neglect the self-potential of any structure they create. Furthermore, the Ferrers’ potentials, although the best of all the available analytical bar potentials, have a number of shortcomings, the most important one for our particular application being that the force they create diminishes too rapidly at large radii. The other potentials we used, although they lack this particular drawback, are ad hoc, and therefore not necessarily realistic. The above remarks should be kept in mind when assessing our quantitative comparisons. Our aim in such cases was to find whether the potentials we used give results in agreement with observations, or, in case of disagreement, whether any obvious and straightforward changes of the potential can bring agreement.

For the outer ring our analysis concentrates on R_1 cases, for which we have sufficient models to reach safe conclusions. With all the potentials used so far, the outer ring shape is in good agreement with observations. Most models are within one σ from the observed mean and all are within two σ . We tried different changes of the potential – such as different rotation curves, adding a lens, or stabilising the L_1 and L_2 Lagrangian points (see Paper III) – and this result remained unchanged. There is thus excellent agreement between model and observed outer ring shapes.

For the inner ring, we found several models with inner ring shapes more elongated than observed. Examining by eye these cases, we found that for most, if not all, the inner manifolds correspond more to the outer regions of the bar and not to the inner ring. We can thus conclude that there is a fair agreement between theory and observations regarding the inner ring axial ratio.

Finally, the ratio of outer to inner ring major axes gives good agreement for some types of models, but not for all. Thus all pseudo-ring cases (rR'_1), independent of the model potential, give good agreement. This is the case also for both rR_1 and rR'_1 morphologies in models with a circular velocity curve showing a slight decrease at or somewhat beyond corotation, for models with stable L_1 and L_2 Lagrangian points and for a number of other models. On the other hand, agreement for cases with an rR_1 morphology and A or AE rotation curves (with or without a lens) often have too small a value of this ratio. It is thus clear that the underlying potential plays an important role. Our calculations suggest that models such that Q_{t,L_1} is somewhat decreased within corotation and increased outside it would give good agreement for all ring size measurements, namely the inner and outer ring shapes (ratio of minor to major axes) and the ratio of the outer to inner ring major axes. It is, however, beyond the scope of this paper to find a model achieving this at all relevant radii, thus includes the best parts of all the models considered, particularly since this exercise may prove futile if self-consistency is taken into account.

We find a trend between the ring axial ratio and the relative

amplitude of the non-axisymmetric forcing in the region around, or immediately beyond corotation, in the sense that stronger bars are linked with more elongated rings. This is true for both inner and outer rings. There is also a trend between the ratio of outer to inner ring major axes and this measure of non-axisymmetric forcing. If we focus on only one model family, or a couple of them, these trends can become clear correlations, but including all models broadens them, sometimes substantially.

In Paper V, the next and last paper of this series, we will present a number of other comparisons with observations and predictions, including kinematics, bar shape, radial drift and abundance gradients. We will discuss pattern speed prediction and give a global appreciation of the application of our theory to observed spirals and rings. We will also consider the effects of time evolution and of self-consistency. Finally we will discuss other theories and simulations and how they link to this work.

ACKNOWLEDGEMENTS

EA thanks Scott Tremaine for a stimulating discussion on the manifold properties. We also thank Ron Buta for useful discussions and email exchanges on the properties of observed rings and for allowing us to reproduce images of two galaxies in Fig. 2 and the anonymous referee for a careful reading of the manuscript. This work was partly supported by grant ANR-06-BLAN-0172 and by the Spanish MCyT-FEDER Grant MTM2006-00478. This paper made use of two images from the Digital Sky Surveys which were produced at the Space Telescope Science Institute under the U.S. Government Grant NAG W-2166.

REFERENCES

- Athanassoula, E. 1980, *A&A*, 88, 184
- Athanassoula, E. 1984, *Phys. Rep.*, 114, 319
- Athanassoula, E. 1992a, *MNRAS*, 259, 328
- Athanassoula, E. 1992b, in ‘Morphological and Physical Classification of Galaxies’, eds. G. Longo, M. Capaccioli & G. Busarello, Dordrecht:Kluwer, Astr. & Sp. Sc. Library, 178, 127
- Athanassoula, E., Bienaymé, O., Martinet, L., Pfenniger, D. 1983, *A&A*, 127, 349
- Athanassoula, E., Bosma, A. 1985, *Ann. Rev. Ast. Astrophys.* 23, 147
- Athanassoula, E., Bosma, A., Crézé, M., Schwarz, M.P. 1982, *A&A*, 107, 101
- Athanassoula, E., Romero-Gómez, M., Bosma, A., Masdemont, J.J. 2009b, *MNRAS*, submitted (Paper V)
- Athanassoula, E., Romero-Gómez, M., Masdemont, J.J. 2009, *MNRAS*, 394, 67 (Paper III)
- Barbanis, B., Woltjer, L. 1967, *ApJ*, 150, 461
- Binney, J., Merrifield, M. 1998, *Galactic Astronomy*, Princeton Univ. Press, Princeton
- Binney, J., Tremaine, S. 2008, *Galactic Dynamics*, Princeton Univ. Press, Princeton, 2nd edition
- Buta, R. 1986, *ApJ*, 61, 609
- Buta, R. 1995, *ApJS*, 96, 39
- Buta, R., Block, D. L., Knapen, J. H. 2003, *AJ*, 126, 1148
- Buta, R., Combes, F. 1996, *Fund. Cosmic Phys.*, 17, 95
- Buta, R. J., Corwin, H. G., Odewahn, S., C. 2007, *The de Vaucouleurs Atlas of Galaxies*, Cambridge University Press.
- Buta, R., Crocker, D.A. 1991, *AJ*, 102, 1715

- Buta, R., Laurikainen, E., Salo, H. 2004, *AJ*, 127, 279
- Buta, R., Vasylyev, S., Salo, H., Laurikainen, E. 2005, *AJ*, 130, 506
- de Vaucouleurs, G. 1959, in *Hanbuch der Physik*, 53, 275
- Dehnen, W., 2000, *AJ*, 119, 800
- Durbala, A., Buta, R., Sulentic, J. W., Verdes-Montenegro, L. 2009, *MNRAS*, 397, 1756
- Eskridge, P.B., Frogel, J.A., Podge, R.W., Quillen, A.C., Davies, R.L., DePoy, D.L., Houdashelt, M.L., Kuchinski, L.E., Ramírez, S.V., Sellgren, K., Terndrup, D., Tiede, G.P. 2000, *AJ*, 119, 536
- Ferrers N. M. 1877, *Q.J. Pure Appl. Math.*, 14, 1
- Frei, Z., Guhathakurta, P., Gunn, J., Tyson, J.A., 1996, *AJ*, 111, 174
- Gadotti, D., 2009, *Chaos in Astromy*, G. Contopoulos and P. Patsis (eds), Springer Verlag, Berlin, 159
- Gómez, G., Koon, W.S., Lo, M. W., Marsden, J. E., Masdemont, J. J., Ross, S. D. 2004, *Nonlinearity*, 17, 1571
- Jörsäter, S., van Moorsel, G. A. 1995, *AJ*, 110, 2037
- Koon, W. S. Lo, M. W., Marsden, J. E., Ross, S. D. 2000, *Chaos*, 10, 2, 427
- Kormendy, J. 1979, *ApJ*, 227, 714
- Kuz'min, G. 1956, *Astron. Zh.*, 33,27
- Laurikainen, E., Salo, H., Buta, R. 2004, *ApJ*, 607, 103
- Laurikainen, E., Salo, H., Buta, R., Vasylyev S. 2004, *MNRAS*, 355, 1251
- Lin, C. C. 1967, *ARA&A*, 5, 453
- Lin, C. C., Yuan, C., Shu, F. H. 1969, *ApJ*, 155, 721
- Lindblad, P. A. B., Lindblad, P. O., Athanassoula, E. 1996, *A&A*, 313, 65
- Lyapunov, A. 1949, *Ann. Math. Studies*, 17
- Lynden-Bell, D., Ostriker, J. P. 1967, *MNRAS*, 136, 293
- Puerari, I., Block, D. L., Elmegreen, B. G., Frogel, J. A., Eskridge, P. B. 2000, *A&A*, 359, 932
- Rautiainen, P., Salo, H., Buta, R., 2004, *MNRAS*, 349, 933
- Romero-Gómez, M., Masdemont, J.J., Athanassoula, E., García-Gómez, C. 2006, *A&A*, 453, 39 (Paper I)
- Romero-Gómez, M., Athanassoula, E., Masdemont, J.J., García-Gómez, C. 2007, *A&A*, 472, 63 (Paper II)
- Romero-Gómez, M., Masdemont, J.J., García-Gómez, C., Athanassoula, E. 2008, *Communications in Nonlinear Science and Numerical Simulations*, 14, 4123, 2009
- Sandage, A. 1961, *The Hubble Atlas of Galaxies* (Washington: Carnegie Institution)
- Schwarz, M. P. 1984, *MNRAS*, 209, 93
- Schwarz, M. P. 1985b, *Proc. ASA*, 6, 202
- Skokos, Ch., Patsis, P. A., Athanassoula, E., 2002, *MNRAS*, 333, 847
- Stock, J., 1955, *AJ*, 60, 216
- Toomre, A., 1963, *ApJS*, 138, 385
- Toomre, A., 1977, *ARAA*, 15, 437
- Toomre, A., 1981, in 'The structure and evolution of normal galaxies', S. M. Fall & D. Lynden-Bell (eds), *Proc. of the Advanced Study Institute*, Cambridge, England, Cambridge University Press, Cambridge and New York, 111